Title
Femtosecond x-ray spectroscopy of an electrocyclic ring-opening reaction.

Journal
Science (New York, N.Y.), 356(6333)

ISSN
0036-8075

Authors
Attar, Andrew R
Bhattacherjee, Aditi
Pemmaraju, CD
et al.

Publication Date
2017-04-01

DOI
10.1126/science.aaj2198

Peer reviewed

REPORT

CHEMICAL PHYSICS

Femtosecond x-ray spectroscopy of an electrocyclic ring-opening reaction

Andrew R. Attar,[1,2] Aditi Bhattacherjee,[1,2] C. D. Pemmaraju,[3,4] Kirsten Schnorr,[1,2] Kristina D. Closser,[3] David Prendergast,[3] Stephen R. Leone[1,2,5]*

The ultrafast light-activated electrocyclic ring-opening reaction of 1,3-cyclohexadiene is a fundamental prototype of photochemical pericyclic reactions. Generally, these reactions are thought to proceed through an intermediate excited-state minimum (the so-called pericyclic minimum), which leads to isomerization via nonadiabatic relaxation to the ground state of the photoproduct. Here, we used femtosecond (fs) soft x-ray spectroscopy near the carbon K-edge (~284 electron volts) on a table-top apparatus to directly reveal the valence electronic structure of this transient intermediate state. The core-to-valence spectroscopic signature of the pericyclic minimum observed in the experiment was characterized, in combination with time-dependent density functional theory calculations, to reveal overlap and mixing of the frontier valence orbital energy levels. We show that this transient valence electronic structure arises within 60 ± 20 fs after ultraviolet photoexcitation and decays with a time constant of 110 ± 60 fs.

The light-activated electrocyclic ring-opening of the 1,3-cyclohexadiene (CHD) chromophore is responsible for a crucial step in the photobiological synthesis of vitamin D_3 in the skin (*1*–*3*) and underlies numerous optoelectronic applications in optical switching (*4*), photochromic devices (*5*), and nanomechanical motors (*6*). The photoinduced isomerization of this particular chromophore has also played a critical role in the development and corroboration of the Woodward-Hoffman rules that govern the stereochemical fate of pericyclic reactions (*7*, *8*) more generally. The reaction scheme of photochemical pericyclic reactions is postulated to involve nonadiabatic transit through an intermediate excited state of the same symmetry as the electronic ground state, implicating a complex interplay between nuclear and electronic degrees of freedom (*9*). Serving as a model of this ubiquitous process, the photoinduced ring-opening of CHD has been the subject of extensive experimental and theoretical investigations (*10*–*14*), which have provided the currently developed mechanism presented schematically in Fig. 1A.

Following ultraviolet (UV) photoexcitation to a 1B excited state via a strong symmetry-allowed $\pi \rightarrow \pi^*$ transition, the photochemical ring-opening reaction is thought to proceed to a dark 2A excited state (*11*) near a surface crossing, or conical intersection, between the 1B and 2A states (labeled CI1) after ~55 fs (*12*, *13*) and, subsequently, through the so-called pericyclic minimum in this intermediate state (*11*). From an electronic structure perspective, the 2A state can be described by a doubly excited electronic configuration, as shown in the intermediate orbital diagram in Fig. 1B (*9*, *14*). According to recent simulations (*15*), the strict separation into a bright 1B state and a dark 2A state may not be exact; however, this labeling convention conveniently differentiates the characteristically distinct regions of the excited-state potential energy surface. As the wave packet moves along the reaction coordinate with concurrent conversion of the photon energy into nuclear dynamics, a reduction in the π-π^* splitting is expected near the pericyclic minimum, consistent with the narrowing gap between the ground- and excited-state potential energy surfaces. In this region, a conical intersection between the 2A excited-state and 1A ground-state potential energy surfaces (CI2) provides the critical outlet for the wave packet to undergo nonadiabatic relaxation onto the 1A transition state region (*11*, *14*). From here, the wave packet bifurcates toward either the 1,3,5-hexatriene (HT) photoproduct or back toward the ring-closed CHD (*13*, *15*). The arrival time at the initial ring-opened HT photoproduct has been previously reported to be ~140 fs (*12*, *14*). A key to understanding this photochemical mechanism, which involves rapid exchange between electronic and nuclear motion, is to directly characterize both the time-evolving molecular structure and the coupled evolution of the valence electronic structure, especially through the crucial intermediate excited state.

Although time-resolved spectroscopic studies have allowed temporal tracing of the excited-state dynamics (*10*, *12*–*14*) and recent femtosecond x-ray scattering experiments have even revealed the time-evolving molecular structure directly (*16*), a direct characterization of the transient valence electronic structure in the intermediate excited-state region has remained elusive. Here, we report femtosecond soft x-ray absorption spectroscopy near the carbon K-edge with spectroscopic analysis from time-dependent density functional theory (TDDFT) calculations of the x-ray spectra to directly reveal the evolution of the valence electronic structure during the photochemical ring-opening reaction in real time. Nonadiabatic molecular dynamics (NAMD) simulations of the entire reaction path were performed and the time-resolved x-ray absorption spectrum (TRXAS) calculated at each time point via TDDFT (*17*).

In general, x-ray absorption spectroscopy is a powerful tool for exploring the electronic structure of molecules with element specificity (*18*) and, when applied with ultrafast pump-probe techniques, can provide detailed information regarding the time evolution of oxidation states, spin states, and chemical environments of specific atomic sites during photoinduced processes (*19*–*29*). Femtosecond x-ray (>100 eV) spectroscopic studies have been mostly restricted to large-facility synchrotrons or free-electron laser sources (*20*, *24*, *25*) and only recently extended to table-top systems (*30*). Here, we used a table-top, high-harmonic x-ray source to probe the UV photoinduced ring-opening reaction of CHD via soft x-ray femtosecond transient absorption spectroscopy near the carbon K-edge (~284 eV), thus demonstrating femtosecond optical pump, x-ray probe spectroscopy on a table-top apparatus. Briefly, a 266-nm pump pulse (4 μJ) was used to photoexcite the CHD molecules to the 1B state by promotion of an electron from the 2π highest-occupied (HOMO) to the $1\pi^*$ lowest-unoccupied (LUMO) molecular orbital, initiating the electrocyclic ring-opening reaction. Broadband soft x-ray pulses (~160 to 310 eV, sub-50 fs) produced via high-harmonic generation (HHG) were used to acquire x-ray absorption snapshots of the reacting molecule in real time (*17*) (figs. S1 and S2). An independent in situ cross-correlation between the UV and soft x-ray pulses was used to find time zero and the instrument response function (IRF) of the experiment, giving a full-width at half-maximum of 120 ± 15 fs (figs. S3 to S5).

In Fig. 2A, the static near-edge x-ray absorption fine structure (NEXAFS) spectrum of CHD is plotted and compared to the corresponding TDDFT calculation. Here, we focus on the pre-edge region of the spectrum (see fig. S6 for the full static NEXAFS spectrum up to 296 eV). The pre-edge resonances, labeled peaks X and Y, each consist of several overlapping transitions into unoccupied molecular valence orbitals. Peak X comprises carbon $1s \rightarrow 1\pi^*$ LUMO transitions localized on the sp^2-hybridized carbon sites; peak Y comprises $1s \rightarrow \sigma^*$(C-C), $1s \rightarrow 2\pi^*$, and $1s \rightarrow \sigma^*$(C-H) transitions (*31*). UV photoexcitation promotes an electron from the HOMO (2π) of CHD to the LUMO ($1\pi^*$), immediately modifying the electronic structure and, therefore, the NEXAFS spectrum. As the potential energy imparted by the photon is converted into kinetic energy of the nuclei, the

[1]Department of Chemistry, University of California, Berkeley, CA 94720, USA. [2]Chemical Sciences Division, Lawrence Berkeley National Laboratory, Berkeley, CA 94720, USA. [3]The Molecular Foundry, Lawrence Berkeley National Laboratory, Berkeley, CA 94720, USA. [4]Theory Institute for Materials and Energy Spectroscopies, SLAC National Accelerator Laboratory, Menlo Park, CA 94025, USA. [5]Department of Physics, University of California, Berkeley, CA 94720, USA.
*Corresponding author. Email: srl@berkeley.edu

electronic structure evolves accordingly, as depicted in Fig. 1B, leading to further changes in the NEXAFS spectrum.

In Fig. 2B, the change in the carbon K-edge NEXAFS spectrum (differential absorption, ΔA) following the 266-nm excitation of CHD is shown as a function of the pump-probe time delay. The differential absorption time scan shown is a representative data set out of four separate data sets collected (other data sets shown in fig. S7). Three distinct temporal windows are marked off in shaded regions of Fig. 2B—namely, 0 to 40 fs, 90 to 130 fs, and 340 to 540 fs—each of which shows a unique differential absorption spectrum corresponding to a different step in the ring-opening reaction. The differential absorption spectra in these three temporal windows are plotted in figs. S8 to S10. To clarify the interpretation of the evolving NEXAFS spectrum, the differential absorption spectra in the three temporal windows are converted to pure "pump on" spectra (i.e., of the photoexcited molecules only) in Fig. 3, A to C, by adding back a scaled "pump off" static spectrum based on the percentage of the molecules in the interaction region that are photoexcited. We estimate the excited percentage from the absorption cross section of CHD at 266 nm (8×10^{-18} cm^2 molecule^{-1}, $\varepsilon = 2000$ liter mol^{-1} cm^{-1}) (*32*) and the pump pulse fluence in the x-ray focus (0.27 mJ mm^{-2}), given the 4-μJ pulse energy (*17*). By this procedure, we estimate that ~13% of the molecules in the soft x-ray focal volume were photoexcited by the UV pump pulse. The static CHD spectrum was scaled accordingly and added to the differential absorption spectrum to obtain the pure "pump on" spectra.

The transient NEXAFS spectra in the 0- to 40-fs, 90- to 130-fs, and 340- to 540-fs time windows are plotted in Fig. 3, A to C, respectively, and compared to the static "pump-off" spectrum. Each transient spectrum is an average over the designated time window. Because of the 120 ± 15 fs IRF, the early time windows of 0 to 40 fs and 90 to 130 fs are not perfectly isolated. In the 0- to 40-fs time window (Fig. 3A), immediately after excitation, we observe a large depletion of the 1π* resonance (peak X), as well as a broad increase in absorption on the low-energy wing (~280 to 284 eV) of peak X and in the valley between peaks X and Y (~286 eV). In Fig. 3B, the most notable transient feature is observed in the 90- to 130-fs time window at ~282.2 eV, which is a new resonance not observed in the NEXAFS of either ground-state CHD or HT (*31*, *33*). Also in this time window, peak Y is broadened and shifts to lower energies, leading to increased absorption amplitude between peaks X and Y. In the final time window (340 to 540 fs in Fig. 3C), which represents the completed reaction, the transient resonance at 282.2 eV has decayed and peak X (1π* resonance) returns completely with even higher amplitude, but is broader and slightly red shifted by ~0.3 eV when compared to the 1π* resonance in the ground-state CHD spectrum. Furthermore, peak Y has shifted back to higher energies. Lastly, in the 340- to 540-fs time window, an increase in absorption in the valley near 289 eV has arisen.

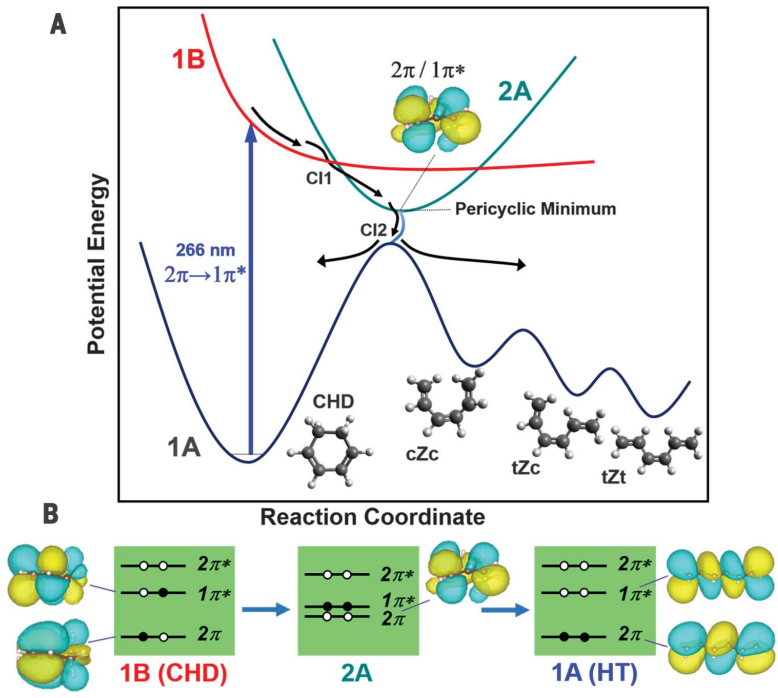

Fig. 1. Electrocyclic ring-opening reaction path. (**A**) Schematic representation showing the relevant potential energy curves along the ring-opening reaction coordinate—modeled after several established schematic figures in the literature (*10*, *12*–*14*). The displayed mechanism is described in the main text. Three conformational isomers of the 1,3,5-hexatriene photoproduct are formed in the reaction, namely s-cis, Z,s-cis (cZc), s-trans,Z,s-cis (tZc), and s-trans,Z,s-trans (tZt) (**B**) Schematic orbital diagram showing the corresponding evolution of the electronic structure (not to scale) of the relevant frontier molecular orbitals at key points along the reaction coordinate. The diagrams represent (from left to right) the 1B state FC region of CHD, the 2A intermediate state, and the 1A state of HT. At the 2A state, near the pericyclic minimum, the 2π and 1π* orbitals are energetically overlapped and mixed, as revealed by the present x-ray spectroscopic results and analysis.

To elucidate the underlying physical processes that govern the evolution of the photoexcited NEXAFS spectrum, we performed NAMD simulations of the reaction to obtain structural and electronic-state information for each time delay relative to UV photoexcitation and calculate the time-resolved carbon K-edge spectra via TDDFT at each time point (Fig. 3, D to F). A total of 116 NAMD trajectories were averaged for each time point to reveal the effects of the vibrational excitation and distribution in nuclear geometries during the reaction. In Fig. 3F, the final reaction trajectories are separated into "successful" (ring-opened) and "unsuccessful" (return to ring-closed ground state) categories, and the x-ray absorption spectra associated with both categories are calculated. Both the ring-opened HT and ring-closed CHD molecules are produced with substantial vibrational energy, which is incorporated in the calculated spectra by the NAMD simulations.

The calculated early time NEXAFS (Fig. 3D) near the Franck-Condon (FC) region of the 1B state shows a depletion and red shift of the 1π* peak X resonance and a new absorption feature at ~280.8 eV, which has carbon 1s→2π character (i.e., into the hole generated in the 2π orbital by 2π→1π* valence excitation). Previous femtosecond time-resolved studies have reported that the movement out of the FC region occurs on an extremely short time scale of ~20 to 30 fs (*12*, *14*). The TDDFT calculations of the x-ray spectra, in combination with the NAMD simulations along the reaction coordinate, show that as the wave packet moves rapidly out of the FC region in the first 40 fs, the 2π and 1π* resonances begin to coalesce around 283.3 eV into near degeneracy (*17*) (fig. S11). As the wave packet moves down the steep 1B potential energy surface, the energy initially imparted by the 266-nm photon in the form of a 2π→1π* excitation (electronic potential energy) is converted to kinetic energy of the nuclei, which lowers the 2π-1π* splitting (schematically illustrated in Fig. 1B). From the perspective of the potential energy surface picture in Fig. 1A, this lowering of the 2π-1π* splitting is represented as the narrowing gap between the ground state and excited state (*17*) (fig. S16), reaching the smallest gap near the pericyclic minimum of the 2A state. Any motion out of the FC region, therefore, will lead to shifting of the 2π resonance from 280.8 eV to higher energies and the 1π* resonance from 284.5 eV to lower energies. This results in the observed broad absorption between ~280 and 284 eV in Fig. 3D, which is an average over the 0- to 40-fs time window.

In Fig. 3A, the experimental transient NEXAFS measured in the 0- to 40-fs time window shows the immediate depletion of the 1π* resonance

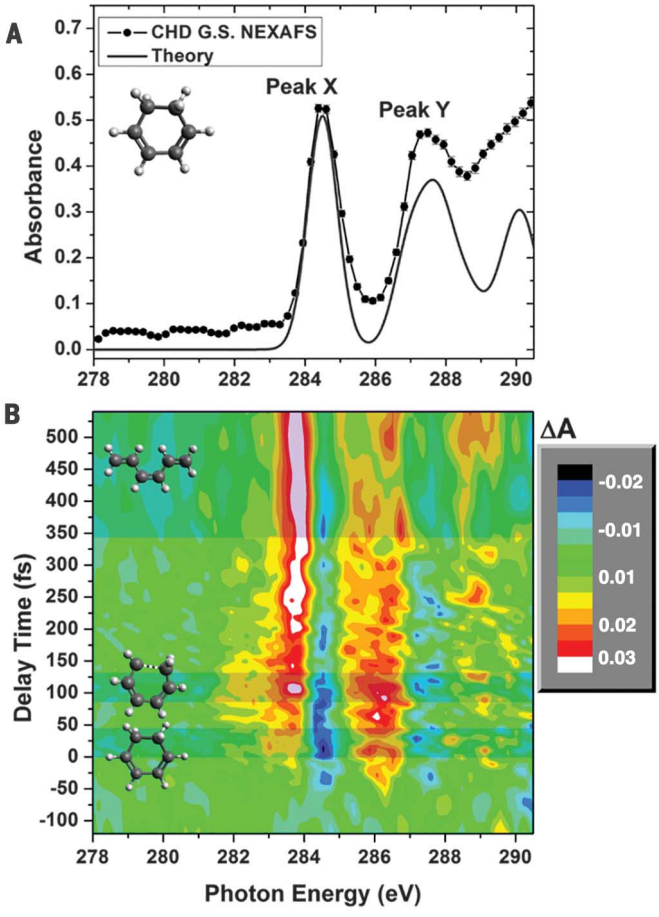

Fig. 2. Static and femtosecond transient absorption spectra of 1,3-cyclohexadiene. (**A**) Comparison of the experimental static NEXAFS spectrum of ground-state (G.S.) CHD (data points shown in full circles connected by solid black line) with the TDDFT calculation for CHD at 300 K (solid gray line). The experimental spectrum is an average of 64 spectra, and the error bars correspond to 95% confidence interval limits. The intensity scale of the calculated spectrum is normalized to peak X in the experimental spectrum. In the TDDFT calculation of the x-ray spectrum, explained in detail in the supplementary materials, a constant 0.4-eV Gaussian broadening was added to each transition. Although the rising nonresonant edge is not included in the calculated spectrum, the relative energies of the pre-edge resonances observed in the experiment are excellently reproduced by the calculation (within 0.1 eV). (**B**) A false-color surface map showing the change in the x-ray absorption (ΔA) as a function of photon energy and delay time, with positive delay times indicating that the soft x-ray pulse follows the UV pulse. An increase in absorption is represented in red or white, a decrease in blue or black. Three temporal windows are indicated by the shaded regions, which each represent an important step in the ring-opening reaction process, as described in the text.

and a broad wing between ~280.5 and 284 eV, in close agreement with the calculated spectrum of Fig. 3D. The broad absorption wing represents the spread of the wave packet out of the FC region toward the 1B/2A conical intersection, in agreement with the calculations for this time window. To observe a continuous shift of the 1s→2π and 1s→1π* resonances, better temporal resolution would be required for the present signal-to-noise levels of this experiment. Nevertheless, we can identify the population dynamics through the 1B state by plotting the time-dependent differential absorption at 284.5 eV (Fig. 4A), where depletion occurs immediately upon UV excitation. The subsequent decay of the depletion at the longest delay times is due to overlapping absorption with the HT photoproducts and vibrationally excited CHD molecules that are produced via internal conversion.

In the TDDFT description, as the system moves away from the FC region on the first-excited potential energy surface, the 2π and 1π* resonances merge into near degeneracy at ~283.3 eV (Fig. 3E, 90- to 130-fs time window). Theoretical analysis of the intermediate resonance at ~283.3 eV reveals that this resonance involves promotion of a carbon 1s electron into a valence orbital of mixed 2π/1π* character (1s→2π/1π*). In the experimental spectrum measured in the 90- to 130-fs time window (Fig. 3B), an intermediate resonance is explicitly observed at 282.2 eV. The ~1-eV discrepancy in the calculated versus experimental energy of this intermediate resonance is tentatively attributed to the inexact treatment of exchange-correlation effects within a single-determinant adiabatic TDDFT description for the 2A state, which has some double excitation character. However, despite the minor discrepancy between theory and experiment in regard to the exact location of the 2π/1π* peak, the merging of the 2π and 1π* resonances in this intermediate region, as predicted by the theory (see also Fig. 2B and fig. S15), is explicitly observed in the experiment. The clear coalescence of the resonance at 282.2 eV provides a direct experimental observation of the elusive 2A state pericyclic minimum and confirmation of the strongly overlapped and mixed 2π and 1π* frontier orbital energy levels in this region.

Because the transient resonance at 282.2 eV represents the signature of the 2A state pericyclic minimum region of the excited-state potential energy surface, the population dynamics through this intermediate region can be represented by the differential absorption at this resonance energy as a function of the pump-probe time delay (Fig. 4B). There is a clear delay between the rise of the 2π/1π* resonance at ~282.2 eV (Fig. 4B) and the depletion of the ground-state CHD 1π* resonance at 284.5 eV (Fig. 4A). The delay corresponds to the time scale required to arrive at the 2A state from the initially excited 1B state FC region and was measured to be 60 ± 20 fs. The subsequent decay of this state was fit to an exponential time constant of 110 ± 60 fs, which corresponds to the lifetime of the 2A state before the wave packet relaxes nonadiabatically through the 2A/1A conical intersection. The error margins in the time constants represent one standard error of the fitted parameter, calculated from the least-squares fitting routine.

Further analysis of the calculated NEXAFS spectrum near the 2A state minimum (Fig. 3E) also reveals a modest (~0.4 eV) red shift of peak Y to ~287.2 eV. The experimental spectrum in the 90- to 130-fs time window of Fig. 3B, in agreement with the theory, shows a ~0.5-eV red shift of peak Y. The red shift observed at peak Y, which involves core transitions to unoccupied orbitals that do not participate in the 266-nm valence excitation, is attributed to nuclear dynamics. In the initial steps of ring opening, the C=C and C-C bonds stretch and the ring is deformed (*12*). Bond elongations lead to red-shifting of core transitions to antibonding orbitals, 1s→σ*(C-C) and 1s→2π*, which underlie peak Y, because of the larger antibonding character of the final core-excited state compared to the valence-excited state (*18*).

Lastly, crossing through the 2A/1A conical intersection along the reactive pathway leads to formation of highly vibrationally excited HT and CHD molecules. In Fig. 3F, as mentioned above, the molecular dynamics trajectories are separated into successful (ring-opened) and unsuccessful (return to ring-closed ground state) categories, and the averaged spectra for both categories are plotted. The large amounts of vibrational excitation of both the ring-opened HT and ring-closed CHD molecules are taken into account in the calculations. The spectrum of the highly vibrationally excited CHD molecule is characterized by a broadening and a strict decrease in amplitude at the resonance center of peak X, compared to the 300 K CHD spectrum. The spectrum of the vibrationally excited HT photoproduct, by contrast, is characterized by a broadening and a strict increase in absorption amplitude at the resonance center of peak X, relative to the 300 K CHD spectrum. The broadening in both spectra is caused by the increased distribution of nuclear geometries in the vibrationally excited molecules, which spreads out the distribution of FC-active vibronic transitions.

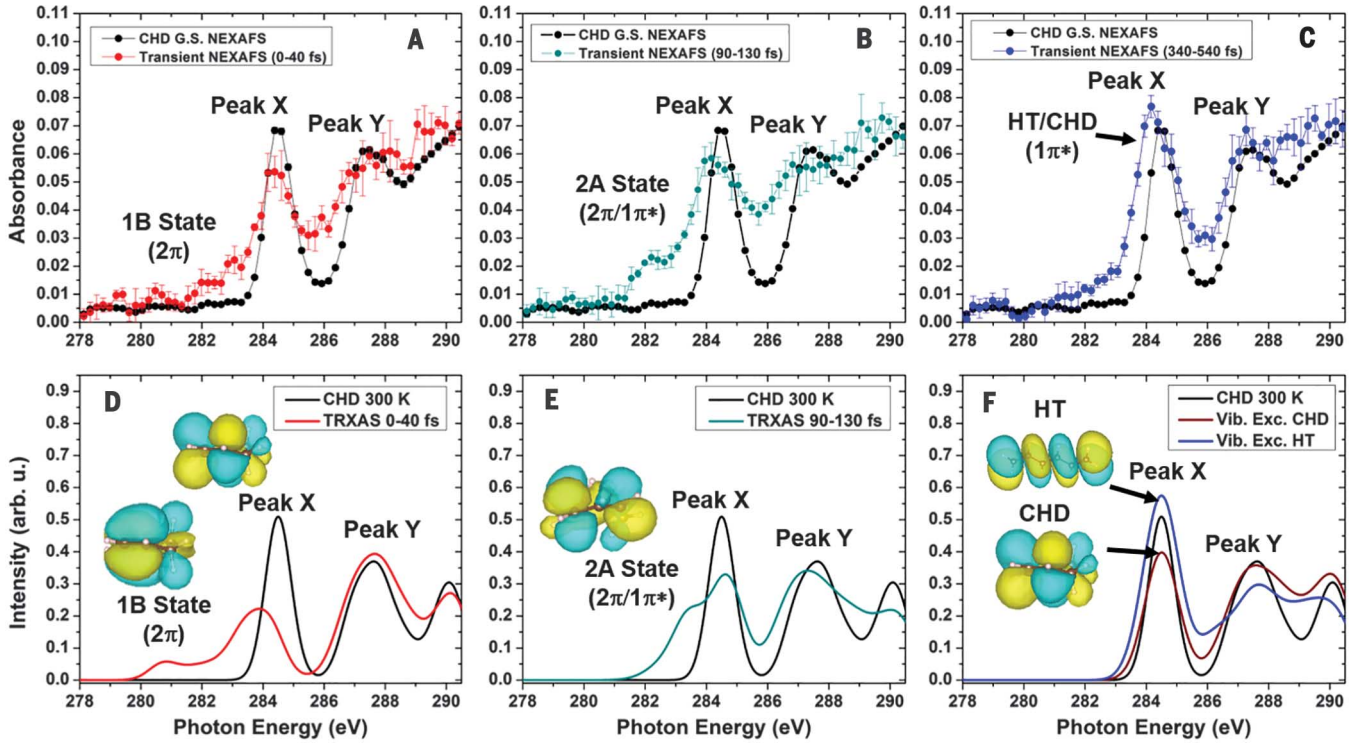

Fig. 3. Experimental and calculated x-ray absorption snapshots. (**A** to **C**) Transient "pump on" x-ray absorption spectra (i.e., of the photoexcited molecules only) measured in the delay-time windows highlighted in Fig. 2B [(A) 0 to 40 fs, (B) 90 to 130 fs, and (C) 340 to 540 fs] and compared to the scaled static x-ray absorption spectrum of ground-state (G.S.) CHD. Each transient spectrum is an average over five time points in the designated time window. For each time point, 32 ΔA spectra are averaged and the error bars correspond to 95% confidence intervals. The error for each time point is propagated in the average of the five time points in each window. As described in the main text, we estimate that ~13% of the molecules in the interaction region were photoexcited. To directly compare the changes in the spectra induced by UV photoexcitation, the static CHD reference spectrum is scaled in accordance with the percent excitation. (**D** to **F**) Calculated x-ray absorption spectra averaged over 116 trajectories of the NAMD simulations: (D) 0- to 40-fs time-averaged spectrum representing the 1B excited-state region, (E) 90- to 130-fs time-averaged spectrum representing the 2A state region, and (F) 340- to 540-fs time-averaged spectra of highly vibrationally excited HT and CHD. The valence orbitals involved in each of the major core-to-valence resonances in the pre-edge regions of the calculated spectra are shown.

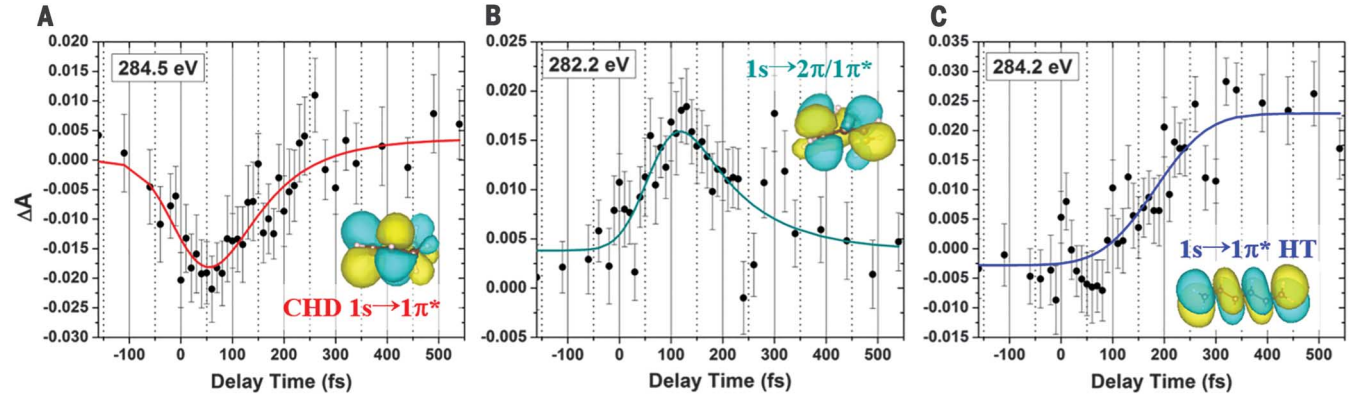

Fig. 4. Time-dependent changes to the x-ray absorption spectrum. Temporal evolution of the differential absorption amplitude (difference between "pump on" and "pump off") at three different x-ray energies. Each differential absorption lineout is an average over 32 measurements, and the error bars in amplitude correspond to 95% confidence intervals. (**A**) Temporal evolution at 284.5 eV, which is the peak energy of the carbon 1s→1π* resonance of ground-state CHD. (**B**) Temporal evolution at 282.2 eV, which is the peak energy of the transient 1s→2π/1π* resonance and therefore represents the dynamics through the intermediate 2A state region near the pericyclic minimum. The lineout is fit to a convolution of the Gaussian IRF with an exponential decay function. The Gaussian width of the IRF (120 fs) is fixed in accordance with the in situ cross-correlation, while all other parameters, including the delayed rise (Δt) and the exponential decay time constant (τ), are free floated. The fit yields $\Delta t = 60 \pm 20$ fs and $\tau = 110 \pm 60$ fs with a coefficient of determination, R^2, of 0.61. (**C**) Temporal evolution at 284.2 eV, representing the peak of the final 1s→1π* resonance of the HT photoproduct. The lineout at 284.2 eV is fit to a delayed rise at 180 ± 20 fs with an R^2 of 0.78. The error margins in all the fitted parameters represent ±1 SE, calculated from the least-squares fitting routine.

Turning to the experimental spectrum measured in the long time-delay limit (340 to 540 fs), the transient spectrum shows a broadening and increase in the absorption amplitude of peak X, as well as a slight red shift, relative to the experimental CHD ground-state spectrum (Fig. 3C).

The key observation in Fig. 3C is the increase in the peak X ($1\pi^*$) amplitude, despite the substantial broadening of the resonance, compared to the CHD ground-state spectrum. The peak X resonance of HT has a larger oscillator strength compared to that of CHD, whereas the peak X amplitude is lower in the spectrum of the vibrationally excited CHD molecules produced via the nonreactive internal conversion (Fig. 3F). Therefore, the overall increase in the observed peak X amplitude in the long time-delay limit of the experiment is caused by the production of ring-opened HT molecules in substantial yield. Further, in the calculated spectra of vibrationally excited HT and CHD (Fig. 3F), an increase in absorption in the valley near 289 eV is predicted in both spectra. Similarly, in the experimental 340- to 540-fs spectrum in Fig. 3C, a new broad absorption feature is observed at ~289 eV, consistent with the calculations.

To address the approximate HT:CHD branching ratio measured in the present investigation, we combined the calculated CHD and HT x-ray spectra in various ratios, searching for the lower limit on the HT:CHD branching ratio that leads to an increase in the peak X amplitude relative to the 300 K spectrum, as observed in the experiment. In this way, the lower limit on the HT:CHD branching ratio was determined to be approximately 60:40. However, this value relies on the relative quantitative oscillator strengths extracted from the calculations, which may not be exact. The NAMD simulations predict a 64% ring-opened population. Although the pre-edge region focused on here offers exceptional sensitivity to changes in valence electronic structure, future experiments using slightly higher soft x-ray energies above the carbon K-edge have the potential to provide higher sensitivity to structural changes through time-resolved extended x-ray absorption fine structure (TREXAFS).

To clock the generation of HT photoproducts, we plot the time-dependent differential absorption lineout at 284.2 eV in Fig. 4C, representing the rise in the peak of the $1\pi^*$ resonance of the HT isomeric mixture, which is red-shifted relative to the ground-state CHD $1\pi^*$ resonance (as seen in Fig. 3C). The lineout reveals a delayed rise at this energy, which reaches an asymptote in the long-time-delay limit and signifies the formation of the ring-opened HT photoproduct. The rise of the HT signal is fit to a delayed step function centered at 180 ± 20 fs.

The analysis of transient carbon K-edge NEXAFS spectra, in combination with NAMD simulations and TDDFT calculations of the TRXAS along the reaction coordinate, thus reveals that the frontier 2π and $1\pi^*$ orbitals are strongly mixed and overlapped near the pericyclic minimum. This transient electronic structure in the intermediate region is consistent with the Woodward-Hoffman framework describing the favorability of a continuous transition of the highest-occupied frontier orbital of the reactant into that of the product (*8*). In photoinduced reactions, the LUMO of the ground-state reactant is the highest-occupied orbital in the excited state, and this orbital is thought to transform into the HOMO of the ground-state product. Providing direct evidence of this intuitive picture, the present results show that the frontier orbitals (i.e., the HOMO and LUMO of ground-state reactant) overlap energetically in the intermediate region between reactant and product, near the critically important pericyclic minimum. With ongoing increases in flux and stability, the continuing application and growing accessibility of water-window soft x-ray pulses on table-top setups promise to expand scientific directions in molecular photochemistry and photophysics.

REFERENCES AND NOTES

1. E. Havinga, R. J. De Kock, M. P. Rappoldt, *Tetrahedron* **11**, 276–284 (1960).
2. E. Havinga, J. L. M. A. Schlatmann, *Tetrahedron* **16**, 146–152 (1961).
3. N. A. Anderson, J. J. Shiang, R. J. Sension, *J. Phys. Chem. A* **103**, 10730–10736 (1999).
4. D. Geppert, L. Seyfarth, R. De Vivie-Riedle, *Appl. Phys. B* **79**, 987–992 (2004).
5. M. Irie, S. Kobatake, M. Horichi, *Science* **291**, 1769–1772 (2001).
6. S. Kobatake, S. Takami, H. Muto, T. Ishikawa, M. Irie, *Nature* **446**, 778–781 (2007).
7. R. B. Woodward, R. Hoffmann, *J. Am. Chem. Soc.* **87**, 395–397 (1965).
8. R. Hoffmann, R. B. Woodward, *Acc. Chem. Res.* **1**, 17–22 (1968).
9. W. T. A. M. Van der Lugt, L. J. Oosterhoff, *J. Am. Chem. Soc.* **91**, 6042–6049 (1969).
10. S. H. Pullen, N. Anderson, L. Walker II, R. J. Sension, *J. Chem. Phys.* **108**, 556–563 (1998).
11. M. Garavelli *et al.*, *J. Phys. Chem. A* **105**, 4458–4469 (2001).
12. K. Kosma, S. A. Trushin, W. Fuss, W. E. Schmid, *Phys. Chem. Chem. Phys.* **11**, 172–181 (2009).
13. B. C. Arruda, R. J. Sension, *Phys. Chem. Chem. Phys.* **16**, 4439–4455 (2014).
14. C. C. Pemberton, Y. Zhang, K. Saita, A. Kirrander, P. M. Weber, *J. Phys. Chem. A* **119**, 8832–8845 (2015).
15. O. Schalk *et al.*, *J. Phys. Chem. A* **120**, 2320–2329 (2016).
16. M. P. Minitti *et al.*, *Phys. Rev. Lett.* **114**, 255501 (2015).
17. See materials and methods in the supplementary materials for details.
18. J. Stöhr, *NEXAFS spectroscopy* (Springer, 1996).
19. W. Gawelda *et al.*, *J. Am. Chem. Soc.* **128**, 5001–5009 (2006).
20. N. Huse *et al.*, *J. Phys. Chem. Lett.* **2**, 880–884 (2011).
21. B. E. Van Kuiken *et al.*, *J. Phys. Chem. Lett.* **3**, 1695–1700 (2012).
22. J. Vura-Weis *et al.*, *J. Phys. Chem. Lett.* **4**, 3667–3671 (2013).
23. J. K. McCusker, *Nat. Phys.* **10**, 476–477 (2014).
24. F. G. Santomauro *et al.*, *Sci. Rep.* **5**, 14834 (2015).
25. H. Öström *et al.*, *Science* **347**, 978–982 (2015).
26. A. R. Attar, A. Bhattacherjee, S. R. Leone, *J. Phys. Chem. Lett.* **6**, 5072–5077 (2015).
27. L. X. Chen, X. Zhang, M. L. Shelby, *Chem. Sci. (Camb.)* **5**, 4136–4152 (2014).
28. X. Zhang *et al.*, *J. Am. Chem. Soc.* **136**, 8804–8809 (2014).
29. B. E. Van Kuiken *et al.*, *J. Phys. Chem. Lett.* **7**, 465–470 (2016).
30. Y. Pertot *et al.*, *Science* **355**, 264–267 (2017).
31. C. Kolczewski *et al.*, *J. Chem. Phys.* **124**, 034302 (2006).
32. F. Rudakov, P. M. Weber, *Chem. Phys. Lett.* **470**, 187–190 (2009).
33. A. V. Teplyakov, A. B. Gurevich, E. R. Garland, B. E. Bent, J. G. Chen, *Langmuir* **14**, 1337–1344 (1998).

ACKNOWLEDGMENTS

This work, A.R.A., and A.B., as well as the materials and a large portion of the equipment, were supported by the U.S. Department of Energy (DOE), Office of Science, Office of Basic Energy Sciences, under contract no. DE-AC02-05CH11231, the gas phase chemical physics program through the Chemical Sciences Division of Lawrence Berkeley National Laboratory (LBNL). K.S. gratefully acknowledges financial support from the Volkswagen Foundation. The apparatus was partially funded by the NSF Engineering Research Center for Extreme Ultraviolet Science and Technology, under a previously completed grant (no. EEC-0310717). Theoretical work by C.D.P, K.D.C, and D.P was performed as part of a User Project at The Molecular Foundry (TMF), LBNL. TMF is supported by the Office of Science, Office of Basic Energy Sciences, of the U.S. DOE, under contract no. DE-AC02-05CH11231. Portions of C.D.P's work integrating nonadiabatic dynamics into transient x-ray absorption spectral simulations were carried out within the Theory Institute for Materials and Energy Spectroscopies at SLAC, supported by the U.S. DOE, Office of Basic Energy Sciences, Division of Materials Sciences and Engineering, under contract no. DE-AC02-76SF00515. Numerical simulations were executed on the Vulcan, Mako, and Lawrencium compute clusters, administered by the High-Performance Computing Services Group at LBNL. All data in both the main manuscript and supplementary materials will be made available upon request.

SUPPLEMENTARY MATERIALS

www.sciencemag.org/content/356/6333/54/suppl/DC1
Materials and Methods
Supplementary Text
Figs. S1 to S17
References (*34*–*64*)

18 September 2016; resubmitted 24 January 2017
Accepted 22 February 2017
10.1126/science.aaj2198

Femtosecond x-ray spectroscopy of an electrocyclic ring-opening reaction

Andrew R. Attar, Aditi Bhattacherjee, C. D. Pemmaraju, Kirsten Schnorr, Kristina D. Closser, David Prendergast and Stephen R. Leone

Science **356** (6333), 54-59.
DOI: 10.1126/science.aaj2198

X-ray vision catches Woodward-Hoffmann

The celebrated Woodward-Hoffmann (W-H) rules rationalize a variety of rapid bond rearrangements in organic molecules. The key insight involved symmetry conservation in the electronic journey from reactant to product. Attar *et al.* now report femtosecond x-ray absorption spectra and accompanying simulation studies that track shifts in carbon electronic states during one such reaction: the photochemical ring opening of cyclohexadiene to hexatriene (see the Perspective by Sension). The smooth evolution that occurs in the vicinity of the pericyclic minimum provides direct affirmation of the W-H framework. Moreover, the use of a convenient tabletop apparatus bodes well for future x-ray studies of ultrafast electronic dynamics.

Science, this issue p. 54; see also p. 31